Fuel 391 (2025) 134602

Contents lists available at ScienceDirect

Fuel

journal homepage: www.elsevier.com/locate/fuel

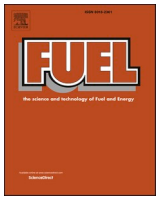

Full Length Article

Evaluation of the influence of different conditions on the Na/Cl release and characteristics of high-alkali coal pyrolysis products by orthogonal and single-factor experiments

Zhihua Tian [1], Bin Zhang [1], Qinhui Wang [*], Ruiqing Jia, Dong Ma, Guilin Xie

State Key Laboratory of Clean Energy Utilization, Zhejiang University, Hangzhou 310027, China

ARTICLE INFO

Keywords:
High sodium and high chlorine coal
Pyrolysis
Migration of sodium and chlorine
Grey relational analysis
Molecular dynamics

ABSTRACT

During the thermal utilization of high-chlorine and high-sodium coal, significant Na and Cl release leads to equipment scaling and corrosion, limiting industrial applications. Pyrolysis, a key pretreatment process, aims to remove these elements before combustion to prevent high-temperature corrosion. Orthogonal experiments efficiently evaluated the effects of multiple factors and their interactions with minimal trials, while grey relational analysis quantified the impact of different conditions on multiple performance indicators, enabling comprehensive optimization of the pyrolysis process. This study identified optimal pyrolysis conditions (500 °C, 0.45—0.90 mm coal particle size, 400 L/h gas flow, CO atmosphere) through orthogonal experiments and grey relational analysis. Under these conditions, char with high reactivity (R = 0.55457) and yield (Y = 71.05 %) was obtained, along with significant Na and Cl release ratios (8.08 % for Na and 77.10 % for Cl). The influence of temperature and atmosphere on the char characteristics and the distribution of Na and Cl forms was further studied by single factor experiments. Temperature significantly influenced Na and Cl distribution and char characteristics. Compared to N_2, non-inert atmospheres (CO and CH_4) altered the structure, reactivity, and ash melting point of the char. Both experimental and molecular dynamics results demonstrate that CO and CH_4 atmospheres enhanced Na release by reacting with insoluble sodium components, while maintaining high Cl release. This research provides insights to reduce corrosion, extend equipment lifespan, and improve high-chlorine and high-sodium coal utilization efficiency in industrial processes.

1. Introduction

The Shaerhu coalfield, located in the eastern Junggar Basin of Xinjiang Province, is the largest integrated coalfield in Asia [1]. Shaerhu coal (SEH) is a low-rank, high-chlorine, and high-sodium coal with substantial reserves [2]. It is characterized by low cost, high calorific value, and high volatile content, offering significant potential for utilization [3,4]. However, the high sodium and chlorine content in SEH poses challenges for its thermal utilization. During combustion, sodium and chlorine are released and deposited on heat exchange surfaces at high temperatures, reducing the heat transfer efficiency of equipment. In addition, these deposits contribute to corrosion and other operational issues [5–7]. Such problems severely impact the normal functioning of equipment, shorten its lifespan, increase maintenance intervals, and raise repair costs, thus limiting the broader application of SEH and other high-sodium coal. Consequently, this study selected pyrolysis, the prevalently adopted pretreatment method, for the experiment. Pyrolysis not only reduces the content of Na and Cl in coal, but also impacts its properties. The reactivity, structure, composition, and ash melting point of char produced by pyrolysis are intimately correlated with combustion efficiency, stability, and pollutant emissions. High-reactivity char can combust more completely, thus improving the utilization efficiency of coal resources. Char with a higher ash melting point can avert slagging problems and ensure stable operation of equipment. By investigating the characteristics of sodium and chlorine release as well as those of char, a better understanding of the behavior of high-sodium and high-chlorine coal in pyrolysis can be achieved. This allows pyrolysis to ensure that the char exhibits favorable properties and simultaneously minimize the sodium and chlorine content in the coal prior to combustion. Consequently, the properties of high-sodium and high-chlorine coal is

* Corresponding author.
E-mail address: qhwang@zju.edu.cn (Q. Wang).
[1] These authors contributed equally to this work.

https://doi.org/10.1016/j.fuel.2025.134602
Received 14 October 2024; Received in revised form 16 January 2025; Accepted 3 February 2025
Available online 13 March 2025

enhanced, and the utilization value of this coal type is increased.

In recent years, numerous studies have attempted to modify sodium and chlorine release using pretreatments or additives to reduce the damage caused by corrosive substances, thereby ensuring safe and stable equipment operation. Pyrolysis is an effective pretreatment method that can alter the release characteristics of sodium and chlorine during the thermal utilization of coal. Wang et al. [8] found that the release of sodium during high-sodium coal pyrolysis occurs primarily between 350 °C and 700 °C. Li et al. [9] investigated the transformation behavior of various sodium forms during pyrolysis, while Zi et al. [10] studied chlorine release at different pyrolysis temperatures. However, these studies have certain limitations. Most studies focus on the effect of a single factor on sodium or chloride release, and few comprehensively consider the combined effect of pyrolysis conditions on product characteristics and sodium/chlorine release. Identifying pyrolysis conditions that simultaneously optimize char characteristics and control Na and Cl release is critical for advancing the industrial application of SEH. This not only improves utilization efficiency but also enhances production safety while reducing maintenance cycles and costs.

Since the combustion process occurs at much higher temperatures than pyrolysis, the release of Na and Cl during combustion can severely affect equipment. Therefore, several researchers have explored methods to enhance Na and Cl release during pyrolysis to minimize their impact during combustion. Huang et al. [11] examined the influence of different pyrolysis heating rates on Na and Cl release, while Yang et al. [12] studied how different sodium forms affect Na and Cl release during pyrolysis. Lv et al. [13] investigated the influence of various atmospheres on sodium and chlorine release during the pyrolysis of high-sodium coal and found that a coal-gas atmosphere can promote Na release. Modifying the pyrolysis atmosphere offers an effective approach to controlling the release of Na and Cl during the pyrolysis of high-sodium coal. This strategy provides a pathway to optimize the pyrolysis process for high-alkali coal, enabling its safe and efficient utilization at reduced costs. However, limited research has been conducted on how different pyrolysis atmospheres influence the migration of sodium and chlorine species or affect the characteristics of char produced from high-sodium coal. To address these gaps and enhance the utilization value of high-sodium coal, it is essential to investigate the mechanisms by which atmospheres impact its pyrolysis behavior.

This study systematically investigates the effects of four pyrolysis conditions (temperature, gas flow, particle size, and pyrolysis atmosphere) on Na/Cl release from SEH and char characteristics, using orthogonal experiments and variance analysis. Additionally, grey relational analysis is employed to evaluate pyrolysis conditions, identifying those that produce high char reactivity and yield while maximizing Na/Cl release. According to the optimal pyrolysis conditions, the influence of single experimental factors on the pyrolysis of SEH is analyzed, and the influence of pyrolysis temperatures and atmospheres on the characteristics and microstructure of char is analyzed. Finally, molecular dynamics simulations are used to explore the reaction mechanisms under different atmospheres.

The novelty of this study lies in the application of grey correlation analysis for a comprehensive assessment of pyrolysis products, thereby determining the optimal pyrolysis conditions, especially the pyrolysis atmosphere. This enables the full exploitation of the advantages of grey relational analysis in the analysis of small-sample, multi-factor, and multi-index systems. It allows for the quantification of the correlation between each factor and the outcome, thereby comprehensively optimizing the pyrolysis process. Subsequently, this research delved into the impacts of temperature and atmosphere on the morphological distribution of Na and Cl, as well as the microscopic characteristics of char, which have received scant attention in prior investigations. Concurrently, the molecular dynamics simulations employed herein probed the mechanism underlying the influence of diverse atmospheres on Na release during pyrolysis. This finding also plugs the research gap regarding mechanism of the influence of pyrolysis atmosphere on Na and Cl release in previous studies. The goal of this study is to alleviate the problems of deposition and corrosion in the utilization of SEH, while enhancing its utilization value, thereby improving the stability of equipment operation and reducing costs, and providing a theoretical basis and technical support for the efficient utilization of SEH and other high-sodium coals.

2. Experimental

2.1. Materials and equipment

The coal used in this experiment was SEH from the Zhundong region of Xinjiang, China. SEH is a low-rank lignite. The proximate analysis and ultimate analysis of SEH are presented in Table 1, while the ash composition is shown in Table 2. Before the experiments, the SEH was ground and sieved into four particle size ranges: 0.90–2.50 mm, 0.45–0.90 mm, 0.30–0.45 mm, and 0.15–0.30 mm. The sieved samples were dried at 105 °C for 12 h in an oven. Take 0.1 g of dried SEH for digestion. After the digestion solution is diluted to 50 mL with deionized water, the Na content in the solution is determined by ion chromatography. The Na content in SEH was 0.82 %. According to GB/T 3558–1996, the Cl content in SEH, determined using the Eschka mixture fusion and potassium thiocyanate titration method, was 0.66 %. The content of different forms of Na and Cl in SEH can be measured by stepwise chemical extraction method, which are summarized in Table 3. The specific details of the stepwise chemical extraction method will be elaborated in subsequent chapters. According to the MT/T 1074–2007 standard, coal with a sodium content greater than 0.5 % is classified as high-sodium coal. According to the GB/T 20475.2–2006 standard, coal with a chlorine content greater than 0.3 % is classified as high-chlorine coal. Since the Na and Cl contents in SEH are 0.82 % and 0.66 % respectively, SEH is classified as high-sodium and high-chlorine coal.

The pyrolysis experiments were conducted using a fluidized bed, as illustrated in Fig. 1. This fluidized bed consisted of a gas supply system, a control system, a reaction system, and a tail gas treatment system. The quartz reactor had a length of 1200 mm, an outer diameter of 50 mm, and an inner diameter of 40 mm, with a maximum operating temperature of 1100 °C. A distributor plate with a pore size of 0.4 mm and a pore spacing of 0.8 mm was installed 50 mm above the bottom of the quartz tube. Before the experiment, the reactor was heated, and the gas was introduced to purge the system. Once the target temperature was reached, the sample was introduced into the reactor. After the set reaction time, the reactor was allowed to cool, and the remaining sample was collected after the quartz tube cooled to room temperature. The sample was weighed and sealed for subsequent analysis.

2.2. Orthogonal experimental design and grey relational analysis

The yield and reactivity of char, along with the release behavior of Na and Cl during coal pyrolysis in a fluidized bed reactor, are significantly influenced by key operational parameters, including pyrolysis temperature, carrier gas flow rate, particle size, and the pyrolysis atmosphere [14,15]. To investigate the char characteristics of SEH under various conditions, orthogonal experiments were conducted based on these four factors. The gases used were N_2, CO_2, CO, and CH_4.

In each pyrolysis experiment, 15 g of SEH was weighed, and the mass was recorded as M_1 (g). Through preliminary experiments, it was found that when the pyrolysis time exceeded 20 min, the product changes were very small. This shows that the coal was completely pyrolyzed within 20 min. In order to explore the effects of pyrolysis atmosphere, temperature, particle size, and carrier gas flow rate on pyrolysis products, the pyrolysis time of each sample was set to 20 min. After the experiment, the char was removed, and weighed again. The mass of the reacted sample was recorded as M_2 (g). The char was ground to a particle size of less than 0.075 mm, and 0.1 g of the char was digested. The digestion solution was diluted to 50 mL with deionized water, and the Na content

Table 1
Proximate analysis and ultimate analysis of SEH.

Sample	Proximate analysis wt.%				Ultimate analysis wt.%					Calorific value(J/g)
	M_{ad}	A_{ad}	V_{ad}	FC_{ad}	C_{ad}	H_{ad}	N_{ad}	S_{ad}	O_{ad}	
SEH	5.04	5.66	43.60	45.70	66.27	5.12	1.01	0.35	16.55	26,635

Table 2
Ash composition of SEH.

Sample	Composition	SiO_2	Al_2O_3	Fe_2O_3	CaO	MgO	K_2O	Na_2O	TiO_2	SO_3	P_2O_5
SEH	wt.%	19.41	13.61	14.48	36.33	2.40	0.34	6.33	0.07	7.02	0.01

Table 3
Contents of different forms of sodium and chlorine in SEH.

Element	Na					Cl		
Content (μg•g^{-1})	Water soluble	Acetic acid soluble	Hydrochloric acid soluble	Insoluble	Total	Water soluble	Insoluble	Total
	5614	211	515	1825	8165	6280	280	6560

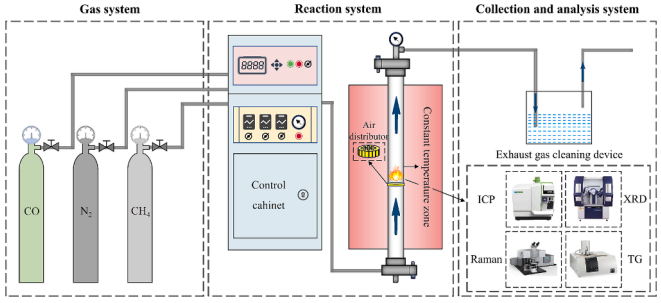

Fig. 1. A fluidized bed reactor.

in the solution was measured using ion chromatography, recorded as n_1 (%). The Cl content in the char was determined according to GB/T 3558–1996, using Eschka mixture fusion and potassium thiocyanate titration, and the Cl content was recorded as c_1 (%). The char yield (Y %), Na release (E_{Na} %), and Cl release (E_{Cl} %) during pyrolysis were calculated using **Formula (1) — (3)**.

$$Y = \frac{M_2}{M_1} \times 100\% \tag{1}$$

$$E_{Na} = \frac{M_1 \cdot n - M_2 \cdot n_1}{M_1 \cdot n} \tag{2}$$

$$E_{Cl} = \frac{M_1 \cdot c - M_2 \cdot c_1}{M_1 \cdot c} \tag{3}$$

The different forms of sodium and chlorine in char were measured using a stepwise chemical extraction method. This method calculates the content of various sodium forms by exploiting their different solubilities in specific solutions [16]. The process involves digesting 1 g of raw coal or char in a microwave digester, diluting the solution to 50 mL, and determining the sodium and chlorine ion concentrations using ion chromatography to obtain the total sodium content (c_N, μg•g^{-1}) and total chlorine content (c_C, μg•g^{-1}). Another 1 g of coal or char is sequentially extracted using deionized deionized water, 1 mol/L ammonium acetate solution, and 1 mol/L hydrochloric acid solution. The extracts are then filtered and diluted to 50 mL, and the sodium ion content (qi, μg/L) in each solution is measured using ion chromatography. This allows the calculation of water-soluble sodium (c_W, μg•g^{-1}), ammonium acetate-soluble sodium (c_A, μg•g^{-1}), and hydrochloric acid-soluble sodium (c_H, μg•g^{-1}), using **Formula (4)**.

$$c_i = \frac{q_i V}{m'} \tag{4}$$

$$c_I = c_N - \sum c_i \tag{5}$$

In **Formula (4)**, M (g) is the mass of the sample used for stepwise extraction or digestion, and V (L) is the volume of the diluted solution. The difference between the total sodium content and the content of each form is used to calculate the insoluble sodium (c_I, μg•g^{-1}), as shown in **Formula (5)**. The determination of water-soluble and insoluble chlorine in coal and char follows the same method as for sodium.

In this study, four factors were evaluated, each with four levels. The experimental factors and levels are presented in Table 4. Based on the factors and levels shown in Table 4, an $L_{16}(4^4)$ orthogonal experimental design was used, with the specific orthogonal experiment table shown in Table 5. This table considers four factors: A (Temperature), B (Gas flow), C (Particle size), and D (Pyrolysis atmosphere).

2.3. Variance analysis in orthogonal experiments

Orthogonal experimental design is an efficient approach for multi-factor, multi-level experiments. It minimizes the number of trials while maximizing the information gained under constrained experimental conditions. This method reduces experimental errors, improving the reliability and precision of the results. Analysis of Variance (ANOVA) is a statistical method used to determine the significance of different factors and their interactions on the experimental outcomes. By comparing between-group variance and within-group variance, ANOVA evaluates the effect of each factor on the response variable and determines whether these effects are statistically significant [17,18]. The steps for variance analysis in orthogonal experiments are outlined below.

Using the orthogonal experimental design, data were collected and organized. The total sum of squares (*SST*), the sum of squares for factors

Table 4
Orthogonal design of experimental factors and levels in pyrolysis.

Level	**Factor A** Temperature (°C)	**Factor B** Gas flow (L/h)	**Factor C** Particle size (mm)	**Factor D** Pyrolysis atmosphere
1	500	300	0.15–0.30	N_2
2	600	350	0.30–0.45	CO_2
3	700	400	0.45–0.90	CO
4	800	450	0.90–2.50	CH_4

Table 5
Orthogonal experimental conditions (L_{16} (4^4)) in pyrolysis.

Case	Factors				Experimental parameter			
	A	B	C	D	Temperature (°C)	Gas flow (L/h)	Particle size (mm)	Pyrolysis atmosphere
1	1	1	1	1	500	300	0.15–0.30	N_2
2	1	2	2	2	500	350	0.30–0.45	CO_2
3	1	3	3	3	500	400	0.45–0.90	CO
4	1	4	4	4	500	450	0.90–2.50	CH_4
5	2	1	2	3	600	300	0.30–0.45	CO
6	2	2	1	4	600	350	0.15–0.30	CH_4
7	2	3	4	1	600	400	0.90–2.50	N_2
8	2	4	3	2	600	450	0.45–0.90	CO_2
9	3	1	3	4	700	300	0.45–0.90	CH_4
10	3	2	2	3	700	350	0.30–0.45	CO
11	3	3	4	2	700	400	0.90–2.50	CO_2
12	3	4	1	1	700	450	0.15–0.30	N_2
13	4	1	4	2	800	300	0.90–2.50	CO_2
14	4	2	3	1	800	350	0.45–0.90	N_2
15	4	3	2	4	800	400	0.15–0.45	CH_4
16	4	4	1	3	800	450	0.15–0.30	CO

(*SSA*), and the sum of squares for error (*SSE*) were calculated. *SST* represents the total variability by measuring the deviation of all data points from the overall mean, as shown in **Formula (6)**. *SSA* reflects the contribution of each factor to the total variability by calculating the squared deviations between each factor level's mean and the overall mean, using **Formula (7)**. *SSE* captures the unexplained variability due to factors not considered in the experiment, calculated with **Formula (8)**.

$$SST = \sum_{i-1}^{n} (x_i - \overline{x})^2 \tag{6}$$

$$SSA_i = \sum_{j-1}^{l_i} n_j \left(\overline{x}_{ij} - \overline{x}\right)^2 \tag{7}$$

$$SSE = SST - \sum_{i=1}^{a} SSA_i \tag{8}$$

In these formulas, x represents the i^{th} observed value, $\overline{x}$ is the overall mean, n is the total number of observations, n_j is the number of observations at the j^{th} level, and $\overline{x}_{ij}$ is the mean for the j^{th} level of i^{th} factor.

Each sum of squares corresponds to a degree of freedom (*DF*), which measures the statistical distribution. The total degrees of freedom (DF_{total}), factor degrees of freedom, and error degrees of freedom (DF_E) are calculated using **Formula (9) — (11)**, respectively.

$$DF_{total} = n - 1 \tag{9}$$

$$DF_{A_i} = l_i - 1 \tag{10}$$

$$DF_E = DF_{total} - \sum_{i=1}^{a} DF_{A_i} \tag{11}$$

Based on these results, the mean squares (*MS*) and the value of *F* were calculated. MS represents the average variation per degree of freedom and is calculated by dividing the sum of squares by the corresponding degrees of freedom. The MS for factors (MS_{A_i}) and the *MS* for error (MS_E) are calculated using **Formulas (12)** and **(13)**, respectively. The value of *F*, the ratio of factor *MS* to error *MS*, is used to assess whether a factor significantly affects the outcome, calculated with **Formula (14)**.

$$MS_{A_i} = \frac{SSA_i}{DF_{A_i}} \tag{12}$$

$$MS_E = \frac{SSE}{DF_E} \tag{13}$$

$$F_{A_i} = \frac{MS_{A_i}}{MS_E} \tag{14}$$

Based on the above results, the contribution of each factor to the dependent variable can be calculated to determine the significant impact of the response variable. The greater the contribution, the stronger the influence of the factor.

2.4. Grey relational analysis (GRA)

Currently, various methods are available for analyzing the correlation between variables, such as grey relational analysis (GRA), regression analysis, response surface methodology (RSM), and multi-objective decision method. Among these, GRA is particularly well-suited for systems with small data sets that involve multiple variables and indicators [19]. By quantifying the relationships between indicators and targets, GRA enables comprehensive optimization, making it an effective tool for solving practical problems with limited data while uncovering underlying patterns and mechanisms.

This study involves multiple evaluation criteria, including yield, reactivity, and the release of Na and Cl, combined with a limited experimental data set derived from orthogonal designs. The capacity of GRA to handle multi-dimensional indicators in such scenarios makes it a particularly appropriate choice. The method simplifies the computational process and offers greater practicality compared to more complex machine learning models. Unlike single-variable regression analysis, GRA does not require extensive assumptions about indicator weights or strict statistical distribution assumptions, which makes it highly adaptable to complex systems with interdependent indicators. Additionally, RSM is more suitable for optimizing continuous variables, whereas GRA excels in the optimization of discrete data. Multi-objective decision-making methods focus on the distance to an ideal solution, while GRA emphasizes the relationships between indicators, providing a more comprehensive understanding of how experimental conditions interact with outcomes. In this study, in order to optimize the pyrolysis conditions, GRA was used to explore the combined effects of various factors (temperature, atmosphere, particle size, and gas flow rate) in the pyrolysis process on the products. The applicability of GRA lies in its ability to handle small sample sizes and multidimensional data, which is very consistent with the orthogonal experimental used in this study. By standardizing the data and calculating the grey correlation, GRA provides a comprehensive assessment of the experimental conditions and can systematically evaluate and determine the optimal pyrolysis conditions. The main steps of GRA are as follows.

Since the factors have different dimensions and scales, the raw data were standardized to eliminate dimensional effects. Range normaliza-

tion was used for this study, with "larger-is-better" and "smaller-is-better" standards calculated using **Formulas (15)** and **(16)**, respectively [20].

$$x' = \frac{x - \min(x)}{\max(x) - \min(x)} \tag{15}$$

$$x' = \frac{\max(x) - x}{\max(x) - \min(x)} \tag{16}$$

In these formulas, x represents the raw data, and x' is the normalized data. After normalization, the grey relational coefficient (*GRC*) between the reference sequence and each comparison sequence was calculated using **Formula (17)**.

$$GRC_i = \frac{\min|x_0 - x_i| + \rho\max|x_0 - x_i|}{|x_0 - x_i| + \rho\max|x_0 - x_i|} \tag{17}$$

In this formula, GRC_i represents the grey relational coefficient for the i^{th} value, x_i is the normalized data, x_0 is the ideal value (the maximum in the normalized data), and ρ is the identification coefficient, typically set at 0.5 [21]. Once the *GRC* is calculated, the grey relational grade (*GRG*) is determined as the average of the *GRC*s, with the GRG_i for the i^{th} experiment calculated using **Formula (18)**.

$$GRG_i = \frac{1}{n}(\mu_1 GRG_1 + \mu_2 GRG_2 + \cdots + \mu_n GRG_n) \tag{18}$$

In this formula, n is the number of characteristics, and μ_n is the weight of each characteristic's *GRC*, where $\sum\mu_n = 1$. A higher GRG_i indicates more optimal performance under the corresponding experimental conditions [22], providing a means of evaluating factor effects and identifying the best controllable factor levels.

2.5. Molecular dynamics simulation

In addition to the experimental investigations, molecular dynamics simulations were carried out to provide a microscopic understanding of the pyrolysis process. Molecular dynamics simulations were performed using the VASP (Vienna Ab-initio Simulation Package) software to investigate the mechanism of atmosphere promoting Na release during the pyrolysis of high-sodium coal. This simulation model incorporated atoms of carbon (C), hydrogen (H), oxygen (O), sodium (Na), silicon (Si), and chlorine (Cl) to represent the key components of the insoluble sodium in high-sodium coal and the relevant species involved in the pyrolysis process.

The generalized gradient approximation with the Perdew-Burke-Ernzerhof (GGA-PBE) functional was employed in the simulations. This function was chosen to accurately describe the electronic interactions and chemical bonding within the system. For the interactions between different atom species, appropriate force field parameters were selected based on the GGA-PBE functional to ensure the reliable calculation of energies and forces. The force field parameters were optimized to account for the specific chemical environment and reactions involved in the pyrolysis process.

A cubic simulation box was constructed. Periodic boundary conditions were applied in all three dimensions of the simulation box. This ensured that the simulated system was effectively infinite in extent, preventing artificial surface effects from dominating the simulation results. The periodic boundary conditions allowed molecules and atoms to freely move across the boundaries of the simulation box. This enabled a more accurate representation of the pyrolysis process as it occurs in a continuous medium, rather than being limited by the boundaries of a finite-sized simulation domain.

Due to the complexity of insoluble sodium compounds in coal (sodium-calcium silicates and sodium-aluminosilicates), Na_2SiO_3 was chosen as a representative compound for energy calculations and transition-state analysis. The initial configuration of the simulation system consisted of Na_2SiO_3 and the gas molecules (CH_4 or CO). The simulations were carried out in multiple steps. First, the adsorption configurations of CH_4 and CO on the Na_2SiO_3 surface were determined by minimizing the total energy of the system. Subsequently, the reaction pathways for the reduction of insoluble sodium under different atmospheres were simulated, the transition states were determined, and the reaction energy barriers were calculated. Finally, the density of states (DOS) of Na_2SiO_3 was calculated to analyze the electronic structure and its influence on the reaction process.

The simulation results, including adsorption energy, reaction pathways, energy barriers, and DOS, were analyzed and compared with experimental data, which provided a deeper understanding of the Na release mechanism in different pyrolysis atmospheres.

3. Results and discussion

3.1. Comprehensive effects of pyrolysis conditions on char

As a pretreatment process, coal pyrolysis operates at a temperature much lower than the combustion temperature, so the Na and Cl released at this stage have relatively little impact on the equipment. Releasing a significant amount of Na and Cl during the pyrolysis of high-sodium coal can lower the concentration of corrosive substances entering the combustion stage, improve char combustion performance, and enhance the stable operation of the equipment. Since Na and Cl release is positively correlated with pyrolysis temperature [14], while char yield and reactivity decrease with increasing temperature [23], achieving high char yield and reactivity alongside substantial Na and Cl release is desirable. This study analyzes the comprehensive effects of pyrolysis conditions to determine the optimal operating conditions that maximize the value of char. Grey relational analysis offers an effective multi-factor approach, enabling a clear evaluation of how different factors influence system performance by calculating their relational degrees. In this study, orthogonal experiments were conducted under four distinct conditions, with grey relational analysis applied.

Using the $L_{16}(4^5)$ orthogonal array, the effects of different pyrolysis temperatures, coal particle sizes, gas flow rates, and pyrolysis atmospheres on char characteristics were studied. In this study, an automatic sampling synchronous thermal analysis system was used to determine the combustion reactivity of char, which is an effective method for measuring the reactivity of char [24,25]. 10 mg of char was weighed each time, and the sample was heated to 1000 °C at a rate of 10 °C/min in an air atmosphere with a flow rate of 100 mL•min^{-1}. The reaction temperature at which the mass loss of char accounts for 50 % of the total mass loss is recorded as $T_{0.5}$, and the reactivity index of char is defined as R. The calculation method of R is shown in **Formula (19)**.

$$R = \frac{(1000 - T_{0.5})}{1000} \tag{19}$$

Fig. 2 shows the char characteristics and results of grey relational analysis under different pyrolysis conditions by the orthogonal experiment. Fig. 2 **(a)** − **(d)** show the yield of char, reactivity of char, release ratio of Na and release ratio of Cl under different pyrolysis conditions, respectively. Fig. 2 **(e)** shows the molar ratio of Na and Cl release under different pyrolysis conditions. Fig. 2 **(f)** shows the results of the air thermogravimetric experiment of char obtained under different pyrolysis conditions. Fig. 2 **(g)** shows the grey correlation coefficient and its ranking for each experiment. Fig. 2 **(h)** shows the average value of the GRG at each level of different influencing factors. Fig. 2 **(a)** shows that, the maximum char yield of 73.78 % occurred at a pyrolysis temperature of 500 °C, particle size of 0.15–0.30 mm, and gas flow rate of 300 L/h, when SEH pyrolysis in the N_2 atmosphere. The char was subjected to a thermogravimetric test in an air atmosphere with a flow rate of 100 mL/min, and the temperature was raised to 1000 °C at a heating rate of 10 °C/min. The experimental results are shown in Fig. 2 **(f)**. The figure shows that the change of the percentage of mass loss in the total mass

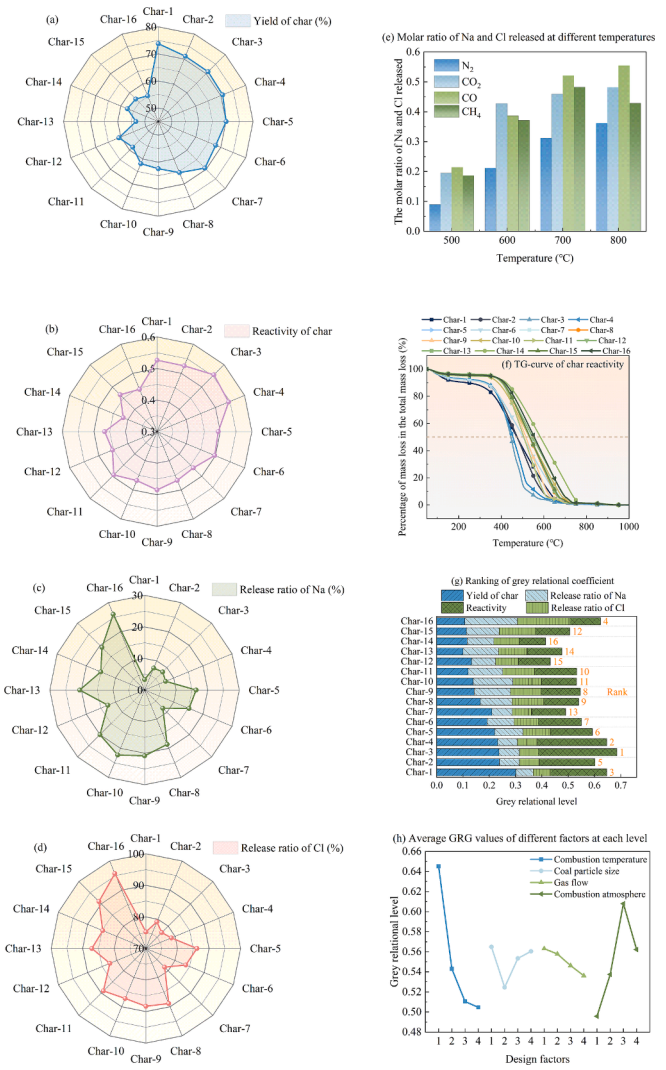

Fig. 2. Char characteristics and grey relational analysis under different pyrolysis conditions: (a) the yield of char, (b) the reactivity of char, (c) the release ratio of Na, (d) the release ratio of Cl, (e) the molar ratio of Na and Cl release, (f) the TG curves of char, (g) the grey correlation coefficient and ranking for each experiment, (h) the average value of GRG at each level of different influencing factors.

loss with increasing temperature. According to the experimental data, the temperature corresponding to the mass loss rate of the char of 50 % is recorded as $T_{0.5}$ (°C) [25]. The larger the R value, the better the reactivity of the char. The reactivity results of the char are shown in Fig. 2 **(b)**.

As can be seen from Fig. 2 **(c)**, when the pyrolysis temperature was 500 °C, Na release remained below 10 %, but at 800 °C, Na release exceeded 15 % across all conditions. The highest Na release of 25.98 % was observed at 800 °C with a particle size of 0.15–0.30 mm and a gas flow rate of 450 L/h, when SEH pyrolysis in the CO atmosphere. As can be seen from Fig. 2 **(d)**, at 500 °C, Cl release surpassed 75 %. The maximum Cl release reached 95.67 %, under the same conditions as the highest Na release. According to Blaesing and Mueller [26], sodium release is influenced by chlorine content. Higher chlorine concentrations favor the formation of alkali metal chlorides. Qi et al. [27] noted that chlorine in coal pyrolysis can also be released in forms other than alkali metal chlorides. As can be seen from Fig. 2 **(e)**, by analyzing the molar ratio of Na and Cl release under the same temperature, it was found that regardless of the temperature, the Na/Cl molar ratio did not exceed 0.6, with Cl released in significantly larger quantities. This indicates that chlorine is not primarily released as NaCl during the pyrolysis of SEH but may also be emitted as HCl(g), KCl(g), Cl_2(g), and other forms.

The primary variables in this study were char yield, reactivity, and the release of Na and Cl. The yield and reactivity of char directly determine the practical value of the obtained char and affect the efficiency of the energy conversion process. In practical applications, high yield and excellent reactivity are key indicators for evaluating char performance. The release of Na and Cl predominantly influence the long-term operational cost of the equipment and are only pertinent to equipment corrosion and maintenance. In order to avoid over-emphasizing equipment maintenance and ignoring product performance, the weights of yield and reactivity are given priority. The methods in previous researches [20,28,29] were referenced. The yield and reactivity should be given higher weights when evaluating the comprehensive characteristics of char. Therefore, the grey relational coefficient weights for yield, reactivity, Na release, and Cl release were set at 0.3, 0.3, 0.2, and 0.2, respectively. **Formulas (15) — (18)** were used to normalize the data, then the grey relational coefficients and grades were calculated for each condition, as shown in Table 6. Higher grey relational grades indicate conditions that yielded char with superior performance, including high yield, reactivity, and Na/Cl release. From Fig. 2 **(g)**, it is evident that char produced under the conditions of *Char-3* had the best overall performance.

According to the result from Table 6, the comprehensive influence of pyrolysis temperature (PT), coal particle size (CS), gas flow rate (GF), and pyrolysis atmosphere (PA) on char yield, reactivity, and Na and Cl release was determined, summarized in Fig. 2 **(h)** and Table 7. The level with the highest average grey relational grade for each experimental factor represents the optimal condition for that factor. The difference between the maximum and minimum average grey relational grades for a factor indicates its overall influence on product characteristics, with a larger difference signifying a greater impact. As shown in Fig. 2 **(h)**, pyrolysis temperature had the highest grey relational grade at 0.645 and the largest range of variation at 0.141, indicating its significant influence on char yield, reactivity, and Na/Cl release. As temperature increased, the grey relational grade for pyrolysis temperature declined, reflecting a diminishing influence on overall char performance. The grey relational grade for pyrolysis atmosphere was 0.608, with a variation range of 0.112, showing that atmosphere also had a significant effect. Notably, the average grey relational grades for pyrolysis atmosphere varied significantly across levels, with CO yielding the best results and N_2 the lowest. This confirms that different pyrolysis atmospheres significantly impact char performance, with CO_2, CO, and CH_4 yielding better results than N_2. This shows that changing the pyrolysis atmosphere can improve quality of the char. The grey relational grade for gas flow rate was 0.565, with a variation range of 0.040. Coal particle size had the least effect, with a grey relational grade of 0.563 and a variation range of only 0.027. The minimal changes in grey relational grades for particle size and gas flow rate indicate that these factors had little impact on overall char performance. Further adjustments to these factors would likely not improve char quality significantly.

To verify the accuracy of the grey relational analysis, ANOVA was conducted on the experimental results, and the findings were compared with those from grey relational analysis. Single-factor ANOVA was performed for char yield, reactivity, and Na/Cl release, with degrees of freedom (*DF*), sum of squares (*SS*), mean squares (*MS*), *F*-values, *P*-values, and contributions (*C*) summarized in Table 8. As shown in Table 8, pyrolysis temperature was the dominant factor influencing char characteristics in pyrolysis, with contributions of 94.21 %, 70.22 %, 66.01 %, and 80.95 %, respectively. This demonstrates that temperature plays a key role in pyrolysis. Pyrolysis atmosphere, as a secondary factor, significantly affected Na release (22.02 %) and Cl release (17.11 %). This is because that CH_4, CO, and CO_2 can participate in coal pyrolysis reactions [30], influencing the breakdown of volatiles and altering the chemical composition of the final products. In contrast, coal particle size and gas flow rate had contribution of less than 5 % for all response

Table 6
Gray relational analysis calculation results.

Normalized data				GRC				GRG	Rank
Y[1]	R[2]	N[3]	C[4]	Y	R	N	C		
1.000	0.797	0.000	0.000	1.000	0.711	0.333	0.333	0.647	3
0.871	0.791	0.186	0.190	0.795	0.705	0.380	0.382	0.602	5
0.867	1.000	0.210	0.091	0.790	1.000	0.388	0.355	0.685	1
0.852	0.933	0.171	0.171	0.772	0.882	0.376	0.376	0.647	2
0.819	0.562	0.573	0.535	0.734	0.533	0.540	0.518	0.592	6
0.716	0.588	0.525	0.414	0.638	0.548	0.513	0.460	0.551	7
0.783	0.335	0.213	0.155	0.698	0.429	0.388	0.372	0.490	13
0.594	0.370	0.675	0.668	0.552	0.442	0.606	0.601	0.540	9
0.447	0.495	0.774	0.640	0.475	0.498	0.689	0.582	0.546	8
0.419	0.373	0.836	0.583	0.463	0.444	0.752	0.546	0.532	11
0.249	0.562	0.737	0.675	0.400	0.533	0.655	0.606	0.532	10
0.365	0.266	0.409	0.348	0.441	0.405	0.458	0.434	0.432	15
0.000	0.360	0.760	0.581	0.333	0.439	0.675	0.544	0.476	14
0.201	0.000	0.516	0.468	0.385	0.333	0.508	0.484	0.414	16
0.172	0.354	0.697	0.773	0.377	0.436	0.622	0.687	0.506	12
0.098	0.209	1.000	1.000	0.357	0.387	1.000	1.000	0.623	4

Note: 1. Yield of char, 2. Reactivity coefficient of char, 3. Release of Na, 4. Release of Cl.

Table 7
Average GRG values for each level.

Phases	PT	GF	CS	PA
1	**0.645**	**0.565**	**0.563**	**0.496**
2	0.543	**0.525**	0.558	0.537
3	0.510	0.553	0.546	**0.608**
4	**0.505**	0.560	**0.536**	0.562
Max.	0.645	0.565	0.563	0.608
Min.	0.505	0.525	0.536	0.496
Deviation	0.141	0.040	0.027	0.112
Rank	1	3	4	2

variables, with *P*-values greater than 0.05, indicating that these factors had no significant effect under the selected experimental conditions.

In this study, the primary objective is to ascertain the most appropriate pyrolysis conditions that can guarantee relatively high yields and reactivities of char, along with significant releases of Na and Cl during pyrolysis. The ANOVA results reveal that when high-sodium coal undergoes pyrolysis in a fluidized bed, temperature and atmosphere have the most profound impacts on the comprehensive properties of the pyrolysis products. By comparing the ANOVA results with those of the GRA, it is evident that the influence of each factor determined by the two methods is highly consistent, thereby validating the reliability of the GRA method employed in this study. Based on the GRA results presented previously, the pyrolysis product characteristics are optimal when the reaction conditions are A1B3C3D3, accompanied by a relatively large amount of Na and Cl released. Therefore, it can be concluded that the optimal pyrolysis conditions for SEH are a temperature of 500 °C, a coal particle size within the range of 0.45——0.90 mm, a gas flow rate of 400 L/h, and a pyrolysis atmosphere of CO.

To verify the reliability of the GRA method, three additional experiments were conducted under the optimal pyrolysis conditions derived from GRA. The results showed consistent performance, with char yields of 73.83 %, 69.26 %, and 68.35 %; Na release ratios of 6.75 %, 10.93 %, and 8.22 %; Cl release ratios of 76.28 %, 81.32 %, and 79.46 %; char reactivity values of 0.5676, 0.5702, and 0.5646, respectively. These results confirm that the char produced under the optimal conditions consistently achieves high yield, reactivity, and significant Na/Cl release, demonstrating the reliability of the optimal conditions derived by GRA. Additionally, to evaluate the choice of CO as the optimal pyrolysis atmosphere, the entropy weight method was applied to analyze

Table 8
ANOVA results of char characteristics.

	Factor	*SS*	*DF*	*MS*	*F*	*P*	Contribution (%)
Yield of char	**PT**	623.778	3	207.926	311.214	0.001	94.206
	GF	4.170	3	1.390	2.081	0.281	0.630
	CS	4.196	3	1.399	2.093	0.280	0.634
	PA	20.850	3	6.950	10.402	0.043	3.149
	Error	2.004	3	0.668	–	–	–
	Total	662.141	15	–	–	–	–
Na release	**PT**	455.845	3	151.948	29.804	0.010	70.224
	GF	3.988	3	1.329	0.261	0.851	0.614
	CS	5.322	3	1.774	0.348	0.795	0.820
	PA	142.933	3	47.644	9.345	0.050	22.019
	Error	15.295	3	5.098	–	–	–
	Total	649.130	15	–	–	–	–
Cl release	**PT**	319.603	3	106.534	10.508	0.042	66.007
	GF	17.553	3	5.851	0.577	0.669	3.625
	CS	11.559	3	3.853	0.380	0.776	2.387
	PA	82.847	3	27.616	2.724	0.216	17.110
	Error	30.414	3	10.138	–	–	–
	Total	484.198	15	–	–	–	–
Reactivity of char	**PT**	0.017	3	0.006	64.638	0.003	80.952
	GF	0.001	3	0.000	3.836	0.149	4.762
	CS	0.000	3	0.000	1.396	0.395	0.000
	PA	0.003	3	0.001	10.338	0.043	14.286
	Error	0.000	3	0.000	–	–	–
	Total	0.021	15	–	–	–	–

the data from orthogonal experiments. The results show that the average comprehensive indicators of N_2, CO_2, CH_4, and CO are 0.37, 0.51, 0.54, and 0.57, respectively. Among them, CO has the highest comprehensive indicators. This shows that the comprehensive performance of char obtained under CO atmosphere is significantly better than that under other conditions, further verifying the rationality of selecting CO to optimize the pyrolysis process. This conclusion informed subsequent single-factor experiments. Through single-factor experiments, the changes in pyrolysis products under CO atmosphere, the effects of various factors, and the potential reaction mechanisms can be deeply studied. Detailed data and calculations for the analysis of entropy weight method are provided in the **Supplementary material**.

3.2. *Effect of single experimental factor on char characteristics*

This study investigates the influence of single experimental factor on char characteristics by altering the pyrolysis conditions. Since coal particle size and gas flow rate exhibited minimal impact on char, these variables were fixed at 0.45–0.90 mm and 400 L/h, respectively, based on optimal conditions. The atmospheres used in this experiment were N_2, CO, CH_4, and CO_2, with pyrolysis conducted at 500 °C, 600 °C, 700 °C, and 800 °C. The char was subjected to a thermogravimetric test in an air atmosphere with a flow rate of 100 mL/min, and the temperature was raised to 1000 °C at a heating rate of 10 °C/min. Fig. 3 **(a)** and **(b)** show the changes in mass fraction of different samples with increasing temperature. Fig. 3 **(c)** shows the char yield under different pyrolysis conditions, while Fig. 3 **(d)** shows the effect of different pyrolysis conditions on the reactivity of char. To determine the reactivity of char, the temperature corresponding to a 50 % loss of total mass must first be determined. This temperature is used together with **Formula (19)** to calculate the reactivity of char [25]. The residual mass of char at 1000°C and its mass fraction can be obtained from the air-TG experimental data. The total mass loss of the sample is equal to the initial mass of the char used in the air-TG experiment minus the residual mass at 1000°C. The sample mass when the mass loss ratio reaches 50 % of the total mass loss can be calculated, and the corresponding temperature $T_{0.5}$ can also be found from the air-TG experimental data. The reactivity of char can then be calculated according to **Formula (19)**. These calculated results are summarized in Table 9.

As Fig. 3 shows, char yield decreases as pyrolysis temperature increases. This occurs because higher temperatures facilitate the more complete decomposition of organic matter, leading to greater volatile release and consequently lower char yield. Compared to N_2, pyrolysis under CO, CH_4, and CO_2 atmospheres produced lower char yields, with CO_2 having the most significant impact at high temperatures. At 800 °C, the char yield in N_2 was 57.53 %, while in CO_2 it dropped to 46.30 %. This reduction is attributed to CO_2 reacting with carbon, initiating gasification and forming CO, resulting in carbon loss. CO also participates in reduction reactions at high temperatures with coal minerals and carbon, generating gaseous products such as CO_2 and CH_4. CH_4 can decompose at high temperatures, converting organic material into gaseous products, further reducing char yield. As seen in Fig. 3 **(d)**, char produced in CO_2 at 500 °C showed the highest reactivity, while char produced in CO displayed the lowest reactivity. The reactivity of char in CH_4 at 500 °C was slightly higher than that in N_2, possibly due to the deposition of hydrocarbon compounds from CH_4 decomposition on the char surface, increasing the concentration of hydrogen-containing functional groups and enhancing reactivity [31]. The reactivity of the char produced under CO atmosphere decreased notably with increasing temperature, as the decomposition of oxygen-containing functional groups and the progressive graphitization of the carbon structure reduced active sites [32,33]. Additionally, pore shrinkage and blockage in char restricted gas diffusion, further lowering reactivity.

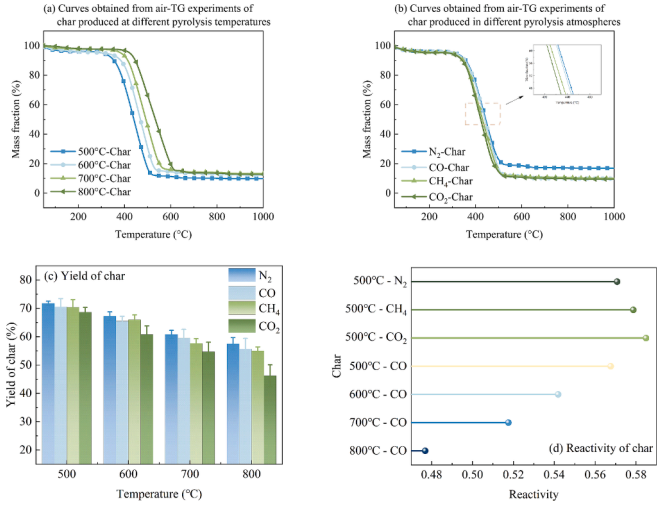

Fig. 3. The yield and reactivity of char produced under different atmospheres and temperatures: (a) curves obtained from air-TG experiments of char produced at different temperatures, (b) curves obtained from air-TG experiments of char produced in different atmospheres, (c) the yield of char, (d) the reactivity of char.

Fig. 4 illustrates the migration and transformation characteristics of Na and Cl in char under various pyrolysis conditions. Fig. 4 **(a)** and **(b)** respectively show the release ratios of Na and Cl when SEH is pyrolyzed at different temperatures and different atmospheres. Fig. 4 **(c)** and **(d)** respectively show the contents of different forms of Na and Cl in the char obtained by SEH pyrolysis at different temperatures and different atmospheres. Regardless of atmosphere, the release ratios of Na and Cl increased with temperature. CO, with its strong reducing nature, disrupts the carbon structure, promoting alkali metal ion migration and release. Na release under CO at 800 °C, reaching 25.94 %. In CH_4 and CO_2, Na release was similar below 700 °C, but at temperatures above 700 °C, Na release under CO_2 increased sharply, reaching 27.04 % at 800 °C. This is because the reduction reaction between CO_2 and carbon ($C + CO_2 \rightarrow 2CO$) accelerates at high temperatures, breaking down the carbon structure and exposing encapsulated Na. When char produced under N_2, Na release remained the lowest, reaching only 16.02 % at 800 °C.

The release of Cl during pyrolysis mainly occurred through chloride volatilization, as Cl desorbed from coal and was released with volatiles [34]. When SEH was pyrolyzed in an N_2 atmosphere at 500 °C, 76.42 % of the chlorine was released, increasing to 86.59 % at 800 °C. The release of Cl generally rises with temperature due to the weakening of physical adsorption between inorganic chlorine compounds (such as NaCl) and the coal matrix, as well as the increased likelihood of chemical bond cleavage at higher temperatures. For organic chlorine, covalently bonded to carbon and hydrogen in coal, higher temperatures provide sufficient energy to overcome bond dissociation energies, promote the decomposition reactions and enhance the Cl release. Pyrolysis atmosphere significantly influences Cl release. At 500 °C, pyrolysis in CH_4, CO, and CO_2 atmospheres increased Cl release by 2.71 %, 2.60 %, and 1.83 %, respectively, compared to N_2. In reducing atmospheres (CH_4, CO), active hydrogen atoms generated by reduction reactions with H_2O can form HCl, enhancing its volatilization. Under weakly oxidizing conditions (CO_2), reactions between CO_2 and the carbon matrix increase porosity and connectivity in char, enabling trapped Cl to escape more easily. Additionally, at higher temperatures, CO_2 can react with alkaline chlorides and chlorine-containing minerals, forming more stable carbonates and destabilizing chlorine compounds, leading to further Cl release [35,36]. At 800 °C, Cl release in a CO_2 atmosphere increased by 9.67 % compared to N_2.

As shown in Fig. 4 **(c)**, in N_2, the water-soluble sodium content in SEH dropped from 5297 $\mu g \bullet g^{-1}$ to 4123 $\mu g \bullet g^{-1}$, while insoluble sodium increased from 1664 $\mu g \bullet g^{-1}$ to 1894 $\mu g \bullet g^{-1}$. Hydrochloric acid-soluble sodium content increased slightly with temperature, indicating that

Table 9
Data obtained from air-TG experiments of char.

	Temperature				Atmosphere			
	500°C	600°C	700°C	800°C	N_2	CO	CH_4	CO_2
Percentage at 1000°C (%)	9.81	12.23	12.74	12.92	16.90	9.81	10.07	9.42
$T_{0.5}$ (°C)	432.38	458.10	482.43	523.12	429.25	432.38	415.12	421.32
Reactivity	0.56762	0.54190	0.51757	0.47688	0.57075	0.56762	0.58488	0.57868

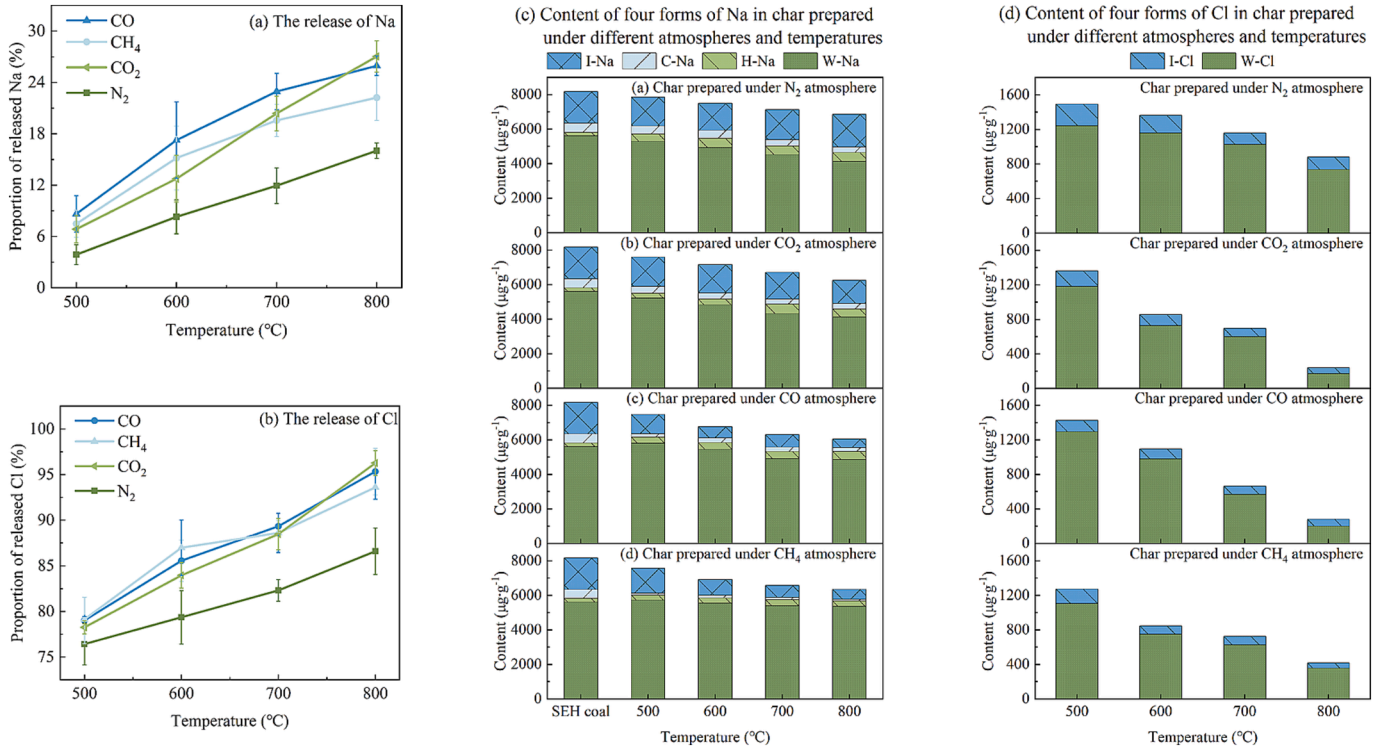

Fig. 4. Release ratios of Na and Cl from char under various pyrolysis conditions and distribution in different forms: (a) the release ratios of Na, (b) the release ratios of Cl, (c) the contents of different forms of Na in the char, (d) the contents of different forms of Cl in the char.

water-soluble Na predominantly volatilizes into the gas phase in N_2. Some water-soluble Na also reacts with unsaturated active sites on the char, forming R-Na structures and increasing hydrochloric acid-soluble sodium [37], while others react with SiO_2, CaO, and Al_2O_3 to form insoluble sodium. Under oxidizing CO_2, water-soluble sodium similarly decreased with rising temperature, but insoluble sodium decreased. CO_2 promotes the dissociation and reorganization of minerals in coal, converting more insoluble sodium into sodium carbonate and other water-soluble forms, which are readily released into the gas phase. In reducing atmospheres, the decline in water-soluble sodium was relatively gradual, whereas the concentration of insoluble sodium exhibited a sharp decrease with increasing temperature. CO and CH_4 can reduce sodium-silicate and sodium-aluminate compounds, breaking Na-Si-O bonds and converting them into metallic sodium or soluble sodium forms. As a result, insoluble sodium content decreased by 72.62 % and 68.01 % under CO and CH_4, respectively, while water-soluble sodium content decreased by only 13.48 % and 4.37 %. The reactions involved are outlined in **R (1) − (7)**.

$$4NaCl + 4CaO + 7SiO_2 \rightarrow 2Na_2Ca_2Si_3O_9 + SiCl_4 \quad R(1)$$

$$4NaCl + 2Al_2O_3 + 5SiO_2 \rightarrow 4NaAlSiO_4 + SiCl_4 \quad R(2)$$

$$SiCl_4 + H_2O \rightarrow HCl + H_2SiO_3 \quad R(3)$$

$$H_2SiO_3 + CaO \rightarrow CaSiO_3 + H_2O \quad R(4)$$

$$NaCl + R\text{-}H \rightarrow R\text{-}Na + HCl \quad R(5)$$

$$Na_2Ca_2Si_3O_9 + CO \rightarrow 2Na + CO_2 + 2CaSiO_3 + SiO_2 \quad R(6)$$

$$3Na_2Ca_2Si_3O_9 + CH_4 \rightarrow 6Na + CO + 2H_2O + 6CaSiO_3 + 3SiO_2 \quad R(7)$$

Reactions **R (1) − (7)** are based on current knowledge of the chemical reactions that can occur between alkali metals and mineral components during coal pyrolysis and on observations made in this study. Similar reactions have been described in previous studies. Reactions **R (1) − (4)**, involving the reaction of NaCl with CaO, Al_2O_3, and SiO_2, are based on studies of common mineral interactions in coal [38–40] and theoretical understanding of the reaction behavior of alkali metal compounds under similar conditions. Complex chemical reactions can occur between these components in pyrolysis to form sodium aluminum silicate and sodium calcium silicate salts. Reactions **R (5) − (7)** were derived from the combination of the phenomena observed in this study and previous studies on the migration of Na forms during the pyrolysis of high-sodium coal [13,40,41]. Through these reactions, different forms of sodium are converted into each other. Combining the basic principles of chemical reactions and referring to previous studies, these reaction equations can be obtained to explain the migration and transformation mechanism of sodium in different atmospheres and its interaction with minerals. This can more intuitively explain the experimental observation of increased Na release in CO and CH_4 atmospheres.

As shown in Fig. 4 **(d)**, both water-soluble and insoluble chlorine contents decreased with increasing temperature across all atmospheres. When coal pyrolysis under N_2 at 500 °C, water-soluble chlorine content

dropped from 6280 μg•g^{-1} to 1245 μg•g^{-1}, a reduction of 80.17 %. At 800 °C, water-soluble chlorine further decreased to 734 μg•g^{-1}, an 88.31 % reduction. Insoluble chlorine, initially at 280 μg•g^{-1}, decreased to 144 μg•g^{-1} at 800 °C, a 48.54 % reduction. The inert nature of N_2 led to lower Cl release, while reducing atmospheres (CH_4 and CO) effectively promoted chlorine release. CO and CH_4 reacted with coal minerals and organics, forming HCl and low-boiling-point compounds such as NaCl and KCl, which volatilized into the gas phase. In CO_2, especially at high temperatures, water-soluble chlorine release became more pronounced. As a weak oxidant, CO_2 promoted the breakdown of organic chlorine and enhanced insoluble chlorine release. At 800 °C, water-soluble chlorine decreased to 71 μg•g^{-1}, a 74.51 % reduction. In summary, CH_4, CO, and CO_2 affect the migration of water-soluble and insoluble chlorine in coal through chemical reactions, increasing Cl release.

The single-factor experiments revealed that, under identical conditions, pyrolysis in a CO atmosphere produces higher char yield and greater release ratios of Na and Cl compared to other atmospheres. This observation corroborates the conclusions from the grey relational analysis, demonstrating the reliability and consistency of both the experimental results and the analytical method used in this study.

3.3. Char characterization and mechanism analysis

The chars produced under various pyrolysis atmosphere and pyrolysis temperature were characterized, as shown in Fig. 6. According to the method proposed by previous researchers, the first-order Raman spectrum from 800 to 1800 cm^{-1} was fitted into ten Gaussian peaks using Peak fit V4.12 software [29,42–44]. The characteristics of carbon materials can be judged based on parameters such as the intensity or ratio of different overlapping peaks. Usually, the G, G_r, V_L, V_r, D and S bands are used to characterize the microstructural characteristics of char. Summary of Raman peak/band assignments were shown in Table 10 [24]. Fig. 5 **(a)** and **(b)** respectively show the Raman spectra of char obtained by SEH pyrolysis at different temperatures and different atmospheres. Fig. 6 **(a)** is a schematic diagram of the peak separation of the char Raman spectrum obtained by SEH pyrolysis in a CO atmosphere at 500 °C. Taking this figure as an example, the remaining char samples were subjected to peak fitting, and the results were calculated and shown in Fig. 6 **(b)** and **(c)**. Fig. 6 **(d)** shows the specific surface area of chars obtained under different pyrolysis conditions. Fig. 6 **(e)** shows the XRD curves of chars obtained under different pyrolysis atmospheres at 500 °C. Fig. 6 **(f)** shows the ash melting characteristic parameters of chars obtained under different pyrolysis atmospheres at 500 °C.

Table 10
Summary of Raman peak/band assignments.

Band name	Band position (cm^{-1})	Description
G_L	1700	Carbonyl group C = O
G	1580–1620	Graphite E^2_{2g}; defect carbon on the aromatic plain of graphite
Gr	1540	Aromatics with 3–5 rings; amorphous carbon structures
V_L	1465	Methylene or methyl; semi-circle breathing of aromatic rings; amorphous carbon structures
Vr	1380	Methyl group; semi-circle breathing of aromatic rings; amorphous carbon structures
D	1320	D band on highly ordered carbonaceous materials; C–C between aromatic rings and aromatics with not less than 6 rings
S_L	1230	Aryl–alkyl ether; *para*-aromatics
S	1180	Caromatic-Calkyl; aromatic (aliphatic) ethers; C–C on hydroaromatic rings; hexagonal diamond carbon sp^3; C–H on aromatic rings
Sr	1060	C–H on aromatic rings; benzene (*ortho*-di-substituted) ring
R	960–800	C–C on alkanes and cyclic alkanes; C–H on aromatic rings

Fig. 6 **(b)** shows that $I_{(Gr+VL+Vr)}/I_D$, I_G/I_D, and I_G/I_{Total} increase with rising temperature, indicating that as temperature increases, the carbon structure transitions from disordered to ordered, with fewer defects and a higher degree of sp^2 carbon ordering. Meanwhile, more small-molecule volatiles are released, and the remaining carbon tends to graphitize. This explains the earlier observation that higher pyrolysis temperatures reduce char reactivity. The value of I_S/I_G decreases with increasing temperature, as sp^3 carbon atoms (CH_2 and CH_3 groups) have lower bond energies at high temperatures and are more prone to dehydrogenation reactions, forming double bonds or aromatic structures. The enhanced conjugation of sp^2 carbon atoms further promotes graphitization. As a result, the aliphatic content in char decreases, while aromatic structures dominate. Under the same pyrolysis conditions, char produced in the CO atmosphere exhibits the highest values of $I_{(Gr+VL+Vr)}/I_D$ and I_G/I_D, indicating that CO promotes the formation of sp^2 carbon. Conversely, CO_2, due to its oxidizing nature, disrupts the carbon structure, leading to more defects and weaker graphitization. The $I_{(Gr+VL+Vr)}/I_D$ and I_G/I_D for char produced in N_2 and CH_4 atmospheres are relatively similar, indicating that both atmospheres exert similar influences on the graphitization process. Although CH_4 is a reducing gas, its chemical reactivity at 500 °C is relatively low, causing it to behave more like an inert gas, similar to N_2. The I_G/I_{Total} values show minimal variation across the four atmospheres, suggesting that while the degree of graphitization differs, the proportion of graphitic structures in char remains relatively unchanged, with only the graphitization degree and defect density varying. The I_S/I_G value of char produced in CO_2 is the highest, indicating a higher aliphatic content, likely due to the oxidizing atmosphere inhibiting graphitization, leaving more aliphatic structures intact. In contrast, char produced in CO has the lowest I_S/I_G value, indicating that CO promotes the formation of sp^2 carbon, reducing aliphatic content and increasing graphitization.

As seen in Fig. 6 **(d)**, when the pyrolysis temperature rises from 500 °C to 600 °C, the S_{BET} increases sharply, reaching a peak of 18.7891 m^2•g^{-1}. This is because during this stage, the release of volatiles from coal increases, creating more internal pores and significantly increasing the surface area. However, after 600 °C, S_{BET} decreases as temperature rises further, dropping to 4.4681 m^2•g^{-1} at 800 °C. This suggests that high temperatures promote the destruction of pore structures, especially in small micropores, where carbon recombination and contraction reduce the surface area. The pyrolysis atmosphere also affects the char surface area. Since N_2 is inert and does not promote the release of volatiles or pore formation, char produced in N_2 has the lowest surface area. In contrast, reducing gases like CH_4 and CO react with oxygen-containing groups on the carbon surface, generating more gaseous products that escape and create additional pores, thus increasing surface area. CO_2 participates in carbonation reactions (CO_2 reacting with carbon to form CO), contributing to pore formation and slightly increasing surface area. However, at 500 °C, CO_2 has low reactivity, so the surface area of char produced in CO_2 is lower than that produced in CH_4 and CO atmospheres.

As shown in Fig. 6 **(e)**, at a pyrolysis temperature of 500 °C, the SiO_2 and CaO peaks are highest in char produced in N_2, while the peaks for SiO_2 and CaO are significantly weaker in char produced in CH_4, CO, and CO_2, with characteristic peaks for calcium feldspar and calcium silicates ($CaAl_2SiO_6$, $Ca_3Al_2SiO_8$, Ca_2SiO_4) appearing. This indicates that in reducing atmospheres (CH_4 and CO) or weak oxidizing atmospheres (CO_2), the mineral components in coal undergo more active reactions, with CaO, Al_2O_3, and SiO_2 to form new silicate and aluminosilicate phases. Additionally, the SiO_2 and $Ca_3Na_2Si_6O_{16}$ peaks are stronger in char produced in N_2 and CO_2 but weaker in char produced in CH_4 and CO, suggesting that reducing atmospheres promote more active reactions between mineral components, with CH_4 and CO likely reacting with some minerals. These reactions form new silicates or lower-grade mineral structures, reducing the relative content of SiO_2 and $Ca_3Na_2Si_6O_{16}$. Meanwhile, the NaCl peak intensity slightly increases, indicating

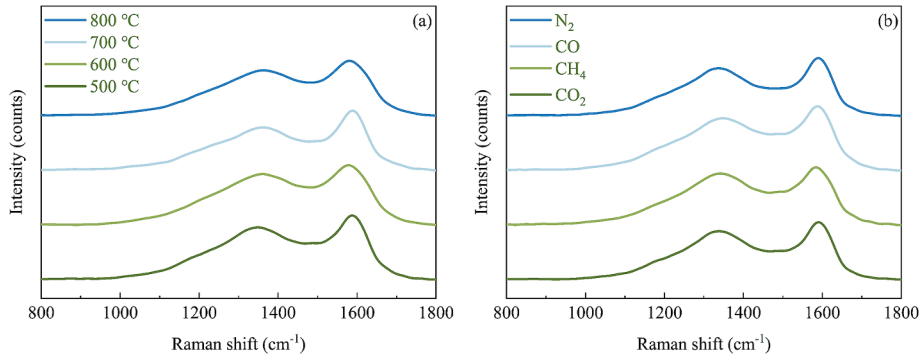

Fig. 5. Raman spectra of char produced by SEH under different pyrolysis conditions: (a) Different temperatures under CO atmosphere, (b) Different atmospheres under 500 °C.

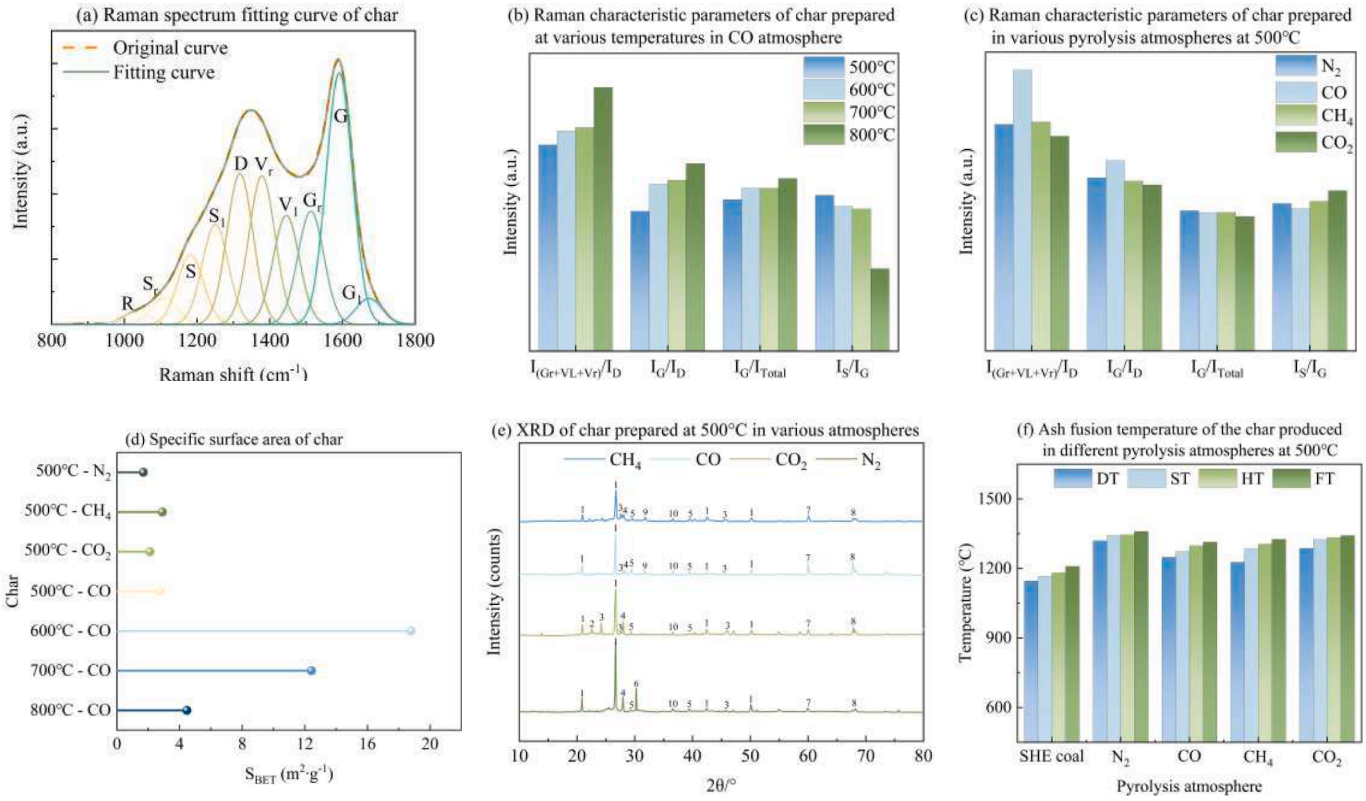

1-SiO_2, 2-$Ca_3Al_2SiO_8$, 3-$CaCO_3$, 4-$Ca_3Na_2Si_6O_{16}$, 5-NaCl, 6-CaO, 7-Al_2O_3, 8-$CaAl_2SiO_6$, 9-Ca_2SiO_4, 10-$Na_2Al_2Si_2O_8$

Fig. 6. Characteristics of char produced under various pyrolysis atmospheres and pyrolysis temperatures: (a) a schematic diagram of the peak separation of the char Raman spectrum obtained by SEH pyrolysis in a CO atmosphere at 500°C, (b) Raman characteristic parameters of char prepared at various temperatures in CO atmosphere, (c) Raman characteristic parameters of char prepared in various atmospheres at 500°C, (d) the specific surface area of char, (e) the XRD curves of char, (f) the ash melting characteristic parameters of char.

that insoluble sodium released through reduction may combine with volatiles to form NaCl, increasing the water-soluble sodium content. This aligns with the earlier finding that char produced in CH_4 and CO has significantly lower insoluble sodium content than char produced in N_2, while water-soluble sodium content is higher. Notably, the $CaCO_3$ peak intensity is significantly higher in char produced in CO_2. This is because CO_2 reacts with calcium (CaO or native calcium minerals) in coal to form $CaCO_3$, inhibiting its decomposition. Overall, CH_4, CO, and CO_2 atmospheres have a significant impact on the mineral composition of char during coal pyrolysis.

As seen in Fig. 6 **(f)**, the ash fusion parameters of char produced in N_2, including deformation temperature (DT), softening temperature (ST), hemispherical temperature (HT), and flow temperature (FT), were the highest, at 1319 °C, 1343 °C, 1345 °C, and 1360°C, respectively. The

ash fusion temperatures of char produced in CO_2 were also high, with DT and ST at 1287 °C and 1325 °C, respectively. However, the ash fusion parameters of char produced in CO_2 is lower than in N_2. This is because CO_2 makes it easier for alkali metals such as sodium and potassium to migrate and transform into low-melting point compounds (carbonates), and react with minerals to form low-melting point complexes. Additionally, the oxidizing nature of CO_2 alters the mineral structure, slightly lowering the ash fusion temperature compared to N_2. Char produced in reducing atmospheres (CO and CH_4) had lower ash fusion temperatures, with DT at 1249 °C in CO and 1227 °C in CH_4. This phenomenon occurs because reducing atmospheres facilitate the reduction of certain oxides or minerals, which subsequently lowers the ash fusion temperature. For example, Fe_2O_3 may be reduced to FeO, and CO and CH_4 may react with minerals to form low-melting-point silicates and carbonates. The ash fusion temperature of SEH was the lowest, with DT at only 1146 °C and FT at 1209 °C, far lower than any char. This indicates that raw coal likely contains more low-melting-point mineral phases, such as chlorides, sulfates, and alkali metal oxides. These mineral components tend to melt and soften at relatively low temperatures when not treated. Fig. 7 illustrates the mechanisms underlying the pyrolysis of high-chlorine, high-sodium coal under different atmospheres.

At present, many scholars have applied molecular dynamics simulation to the mechanism study of reaction processes in multiphase reaction systems [45,46]. To investigate the mechanism by which CH_4 and CO promote Na release during the pyrolysis of high-sodium coal, molecular dynamics simulations were conducted using VASP software with the GGA-PBE functional in this study. This type of simulation method has been widely used in studying coal pyrolysis processes and has been proven to be effective [46–48]. These simulations aimed to explore the kinetics and energy barriers of the reaction process, providing detailed microscopic insights at the atomic and molecular levels. Due to the complexity of insoluble sodium compounds in coal (sodium-calcium silicates and sodium-aluminosilicates), it would be computationally intensive to simulate all these compounds, and fully analyzing their behavior would be challenging. Thus, a simplified approach was necessary. Under high temperatures and specific atmospheres, reactions between reducing gases and insoluble sodium primarily depend on the interaction between sodium and silicon-oxygen groups. Na_2SiO_3, a typical sodium silicate, though chemically and structurally distinct from other insoluble sodium compounds, shares the same Na-O-Si structure and exhibits similar chemical behavior. Therefore, Na_2SiO_3 was chosen as a representative compound for energy calculations and transition-state analysis to reflect the typical behavior of the Na-O-Si system during pyrolysis in reducing atmospheres, providing a deeper understanding of the reasons for changes in insoluble sodium content. The simulation results are shown in Fig. 8. Fig. 8 **(a)** and **(b)** show the adsorption configurations of CH_4 and CO, respectively. Fig. 8 **(c)** and **(d)** show the processes of CH_4 and CO reduction and release of Na (g), respectively. Fig. 8 **(e)** compares the pathway of the reduction reaction of CH_4 and CO. Fig. 8 **(f)** shows the DOS density of states of sodium silicate.

Fig. 8 **(a)** and **(b)** present the most stable adsorption configurations of CO and CH_4 molecules at different sites on the surface of Na_2SiO_3, along with their corresponding adsorption energies. Based on the relevant theories of molecular adsorption and surface interaction in previous studies [49], the adsorption behavior of CH_4 and CO at different sites on the Na_2SiO_3 surface can be better analyzed. CO and CH_4 exhibit negative adsorption energies, indicating spontaneous adsorption on the Na_2SiO_3 surface. CH_4 exhibits adsorption energies of −0.751 eV, −0.496 eV, and −0.125 eV at the Na, O, and Si sites, respectively, while CO exhibits adsorption energies of −0.557 eV, −1.036 eV, and −0.228 eV at the same sites. These results suggest that CH_4 adsorbs most stably at the Na site, while CO prefers the O site.

Fig. 8 **(c)** and **(d)** illustrate the processes by which CH_4 and CO adsorb onto the surface of Na_2SiO_3 and release Na. Upon adsorption, the C–H bond in CH_4 is activated and cleaved, generating $*CH_3$, which serves as an intermediate in subsequent reduction reactions. $*CH_3$ interacts with Na_2SiO_3, forming the unstable intermediate $*CH_3Na$. At high temperatures, the Na-C bond dissociates, leading to the release of Na(g). The $*CH_3$ radical itself is unstable and ultimately undergoes C–H

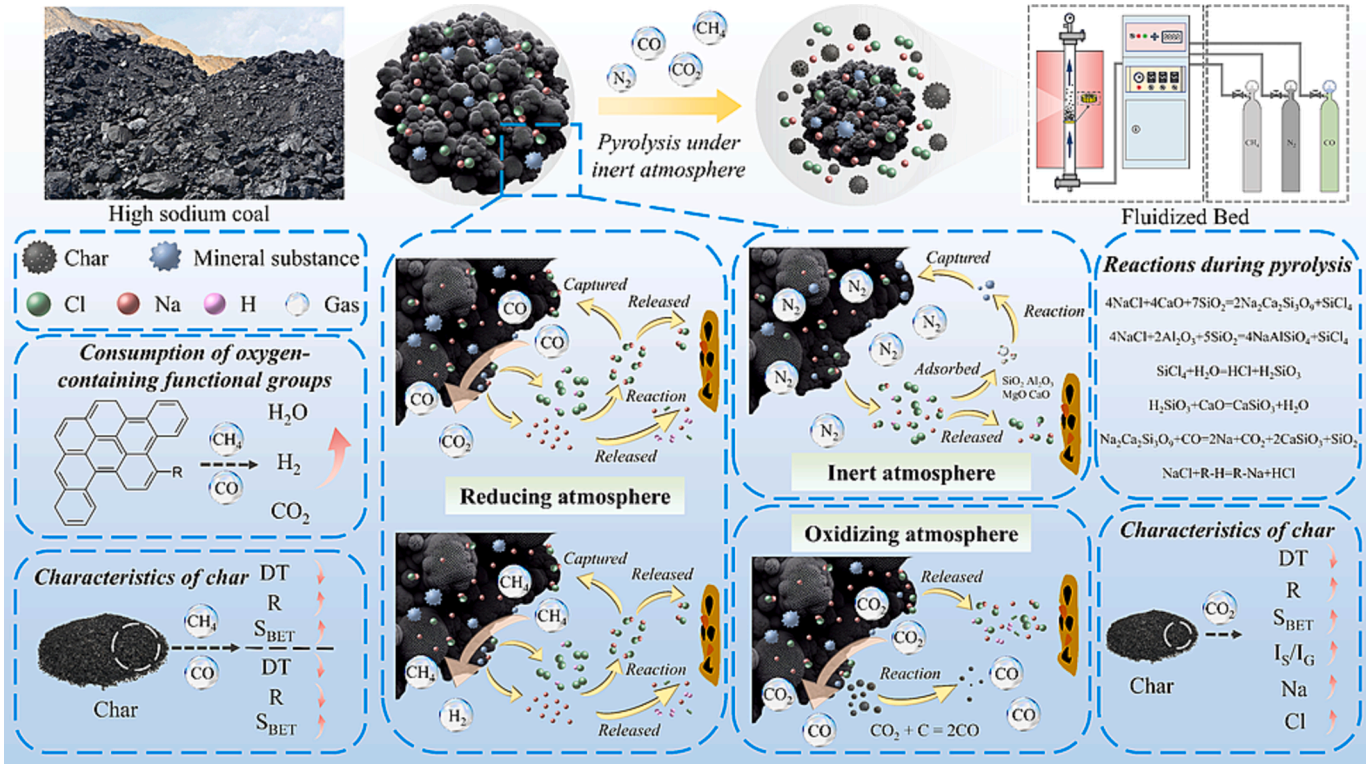

Fig. 7. Mechanism diagram of pyrolysis of high-chlorine and high-sodium coal under different atmospheres.

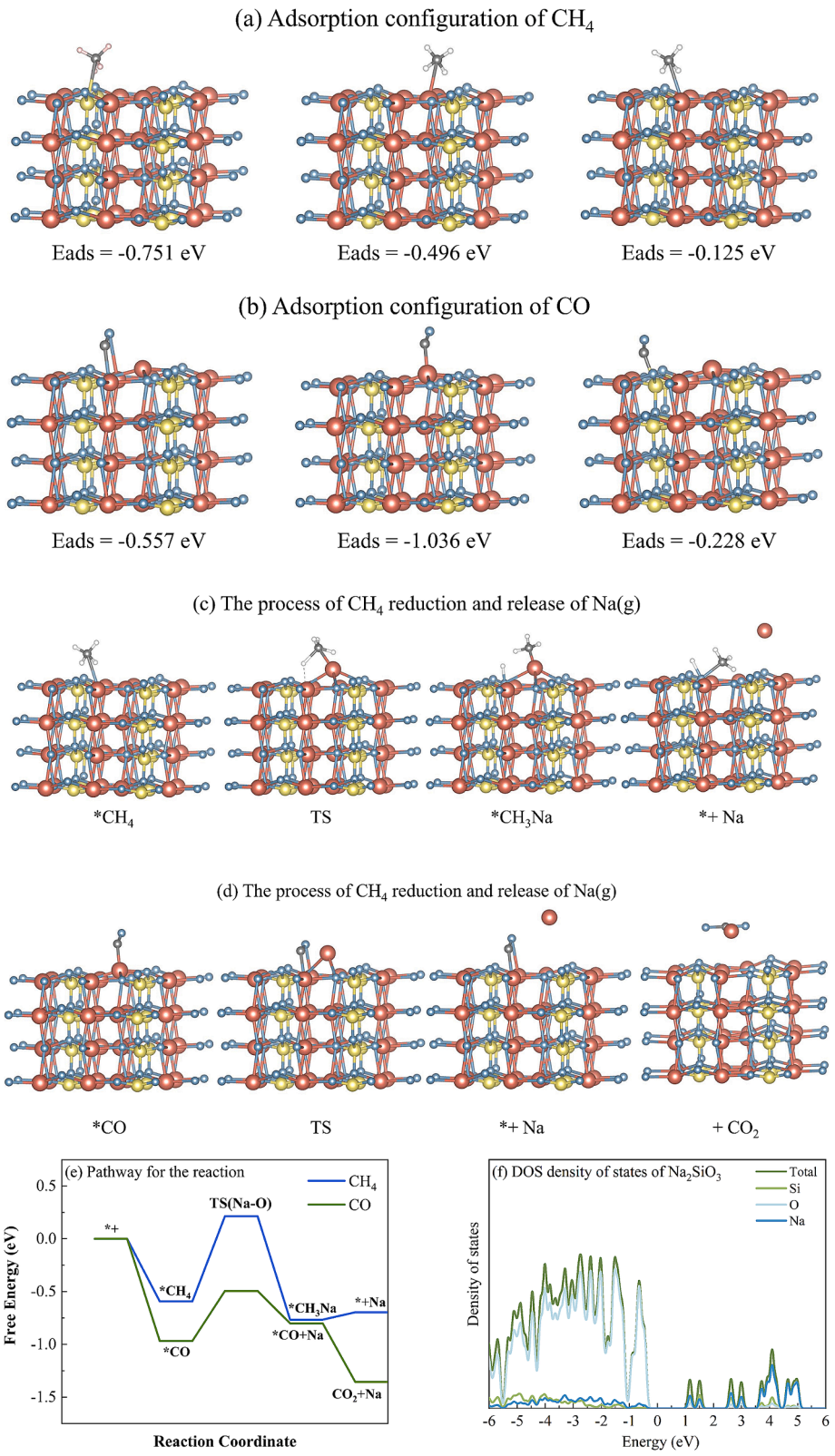

Fig. 8. Molecular dynamics simulation of CH_4 and CO promoting the release of insoluble sodium: (a) the adsorption configurations of CH_4 , (b) the adsorption configurations of CO, (c) the reduction of CH_4 , (d) the reduction of CO, (e) the pathway of the reduction reaction of CH_4 and CO, (f) the DOS density of states of sodium silicate.

bond cleavage, forming gaseous products such as hydrogen or elemental carbon. The SiO_2 remains in the solid phase. For CO, adsorption leads to the breaking of the Si-O bond, producing CO_2 and releasing Na atoms, which migrate to the surface and form Na(g). Thus, through different intermediates and transition states, both CH_4 and CO can promote Na release.

With reference to the calculation methods and related concepts provided by previous studies [50,51], the energy characteristics of the reaction paths under different pyrolysis atmospheres in this study can be better analyzed. Fig. 8 **(e)** shows the microscopic reaction pathways for CH_4 and CO reducing Na-Si-O. The adsorption of both gases is exothermic, forming stable adsorbed states. The transition state (TS) for CH_4 has a higher free energy (about 0.2 eV), indicating a more complex reaction with a higher energy barrier, whereas CO has a lower energy barrier, making it more efficient at releasing Na. The analysis reveals that CO destroy the structure of Na-Si-O more readily during pyrolysis, consistent with the experimental findings of higher Na release under CO.

Fig. 8 **(f)** shows the density of states (DOS) of Na_2SiO_3. Previous studies [52,53] have shown that electronic structure can predict the reduction properties of a substance. The total density of states curve reflects the electronic state distribution in the entire Na_2SiO_3 system. The peak density of electronic states changes significantly near the Fermi level, which shows that the electronic states in Na_2SiO_3 are denser near the Fermi level. This part of electrons is likely to participate in chemical reactions, thereby affecting the reaction process of CH_4 and CO on the surface of Na_2SiO_3. The DOS of Si is concentrated in the lower energy range (−6 eV to −4 eV), indicating minimal participation in high-energy reactions, while the DOS of O in the mid-to-high energy range has a significant distribution (−4 eV to 0 eV) and it coincides with the main peak of the total density of states. This indicates that O atoms play an important role in the Na_2SiO_3 structure and may have a significant impact on chemical reactions and electron transfer processes. The DOS of Na is mainly concentrated in the higher energy level range (3 eV to 5 eV), and has almost no significant contribution below the Fermi level. This indicates that the valence electrons of Na atoms are mainly located in the conduction band and more likely to lose electrons, making it easier for Na to participate in the reaction and be released. This is consistent with the conclusion mentioned above that Na is easily released from Na_2SiO_3 in the high-temperature reducing atmosphere.

The molecular dynamics simulations and experimental data demonstrate strong consistency, reinforcing the reliability of the findings of this research. Experimental results indicate that Na release is significantly higher in CO and CH_4 atmospheres compared to N_2 during pyrolysis. As an inert gas, N_2 does not participate in reactions with components in coal, whereas CO and CH_4 actively promote the cleavage of Na-Si-O bonds. Simulations further reveal that the energy barrier for Na release is lower in CO than in CH_4, aligning with the experimental observation that Na release is more pronounced in a CO atmosphere under identical pyrolysis conditions. This correlation underscores the synergistic use of experimental and simulation methods in elucidating the mechanisms of Na release under varying pyrolysis atmospheres. The agreement between experimental and simulation results enhances the reliability of the study and provides a comprehensive explanation for the enhanced Na release observed in reducing atmospheres.

4. Conclusion

Previous studies have rarely explored the combined effects of multiple factors on the comprehensive characteristics of pyrolysis products. This study systematically evaluated the influence of pyrolysis conditions (temperature, atmosphere, particle size, and gas flow rate) on Na/Cl release and char characteristics using orthogonal experiments with grey relational analysis. Single-factor experiments further investigated the migration mechanisms of Na and Cl under varying atmospheres and temperatures. Additionally, molecular dynamics simulations revealed the microscopic mechanism by which CH_4 and CO promote the release of insoluble sodium, addressing a critical gap in the understanding of pyrolysis atmospheric effects on Na release.

This study identified temperature as the most significant factor affecting Na/Cl migration during pyrolysis, with CO, CH_4, and CO_2 atmospheres enhancing their release through reactions with char components. The optimal pyrolysis conditions were determined (500 °C, 0.45——0.90 mm particle size, 400 L/h flow rate, CO atmosphere). Single-factor experiments showed that non-inert atmospheres produced looser char structures and lower ash melting points, promoting Na/Cl release by 5——15 % and 3——10 %, respectively, compared to inert atmospheres. Molecular dynamics simulations further revealed that reducing gases (CO and CH_4) enhance Na release by adsorbing onto minerals and triggering reduction reactions.

In summary, the optimal pyrolysis conditions identified in this study offer valuable guidance for industrial applications. These conditions enable the production of high-yield, highly reactive char while maximizing Na and Cl release, reducing the corrosion risks in subsequent combustion process, and extending equipment lifespan. Additionally, the findings highlight the effectiveness of CO in enhancing Na release, providing a theoretical basis for selecting suitable pyrolysis atmospheres. Although this study focused on SEH, the methods and results can be adapted to other coal types and industrial scenarios, supporting broader applications in pyrolysis optimization.

CRediT authorship contribution statement

Zhihua Tian: Writing – review & editing, Writing – original draft, Software, Methodology, Investigation, Formal analysis. **Bin Zhang:** Writing – review & editing, Writing – original draft, Methodology, Formal analysis. **Qinhui Wang:** Writing – review & editing, Software, Resources, Project administration, Methodology. **Ruiqing Jia:** Writing – review & editing, Visualization, Data curation. **Dong Ma:** Writing – review & editing, Methodology, Formal analysis. **Guilin Xie:** Software, Investigation, Data curation.

Funding

Thanks for the financial support by the Fundamental Research Funds for the Central Universities (2022ZFJH004).

Declaration of competing interest

The authors declare that they have no known competing financial interests or personal relationships that could have appeared to influence the work reported in this paper.

Acknowledgments

Thanks for the technical and financial support of Dongfang Electric Corporation-Zhejiang University Joint Innovation Research Institute. Thanks for the financial support by the Fundamental Research Funds for the Central Universities (2022ZFJH004).

Appendix A. Supplementary data

Supplementary data to this article can be found online at https://doi.org/10.1016/j.fuel.2025.134602.

Data availability

Data will be made available on request.

References

[1] Wei B, Wang X, Tan H, et al. Effect of silicon–aluminum additives on ash fusion and ash mineral conversion of Xinjiang high-sodium coal[J]. Fuel 2016;181(1):1224–9.

[2] Zhou J, Zhuang X, Alastuey A, et al. Geochemistry and mineralogy of coal in the recently explored Zhundong large coal field in the Junggar basin, Xinjiang province, China[J]. Int J Coal Geol 2010;82:51–67.
[3] Ge H, Shen L, Gu H, et al. Combustion performance and sodium transformation of high-sodium ZhunDong coal during chemical looping combustion with hematite as oxygen carrier[J]. Fuel 2015;159:107–17.
[4] Li G, Li S, Huang Q, et al. Fine particulate formation and ash deposition during pulverized coal combustion of high-sodium lignite in a down-fired furnace[J]. Fuel 2015;143:430–7.
[5] Li R, Kai X, Yang T, et al. Release and transformation of alkali metals during co-combustion of coal and sulfur-rich wheat straw[J]. Energ Conver Manage 2014;83:197–202.
[6] Wang X, Xu Z, Wei B, et al. The ash deposition mechanism in boilers burning Zhundong coal with high contents of sodium and calcium: A study from ash evaporating to condensing[J]. Appl Therm Eng 2015;80(5):150–9.
[7] Wiinikka H, Grönberg C, Öhrman O, et al. Influence of TiO_2 additive on vaporization of potassium during straw combustion[J]. Energy Fuel 2009;23:5367–74.
[8] Wang C, Jin X, Wang Y, et al. Release and Transformation of Sodium during Pyrolysis of Zhundong Coals[J]. Energy Fuel 2015;29(1):78–85.
[9] Li R, Chen Q, Zhang H. Detailed Investigation on Sodium (Na) Species Release and Transformation Mechanism during Pyrolysis and Char Gasification of High-Na Zhundong Coal[J]. Energy Fuel 2017;31(5):5195–202.
[10] Zi J, Ma D, Rahman UZ, et al. Effects of temperature and additives on ash transformation and melting of high-alkali-chlorine coal[J]. Therm Sci 2020;24(3):1271–81.
[11] Huang Z, Li N, Zhou Q, et al. A comparative study of the pyrolysis and combustion characteristics of sodium-rich Zhundong coal in slow and rapid processes[J]. Energy Sci Eng 2018;7(1):98–107.
[12] Yang Y, Lin X, Chen X, et al. Investigation on the effects of different forms of sodium, chlorine and sulphur and various pretreatment methods on the deposition characteristics of Na species during pyrolysis of a Na-rich coal[J]. Fuel 2018;234:309–17.
[13] Lv K, Luo Z, Fang M, et al. Effect of pyrolysis atmosphere on sodium behavior in Zhundong coal and study on slagging characteristics of char[J]. Energy Eng 2022;42(6):1–8.
[14] Dimple MQ, Wu H, Sankar PB, et al. Volatilisation and catalytic effects of alkali and alkaline earth metallic species during the pyrolysis and gasification of Victorian brown coal. Part II. Effects of chemical form and valence[J]. Fuel 2002;81(2):143–9.
[15] Huhn F, Klein J, Jüntgen H. Investigations on the alkali-catalysed steam gasification of coal: Kinetics and interactions of alkali catalyst with carbon[J]. Fuel 1983;62(2):196–9.
[16] Xu L, Liu H, Zhao D, et al. Transformation mechanism of sodium during pyrolysis of Zhundong coal[J]. Fuel 2018;233:29–36.
[17] Lodhi BK, Agarwal S. Optimization of Machining Parameters in WEDM of AISI D3 Steel Using Taguchi Technique[J]. Procedia CIRP 2014;14:194–9.
[18] Song C, Wang H, Sun Z, et al. Optimization of process parameters using the Grey-Taguchi method and experimental validation in TRIP-assisted steel[J]. Mater Sci Eng A 2020;777(10):139084.
[19] Rikos E, Tselepis E, Klick CH, et al. Stability and power quality issues in microgrids under weather disturbances study of photovoltaic integration[J]. IEEE J Sel Top Appl Earth Obs Remote Sens 2008;1(3):170–80.
[20] Üstüntağ S, Şenyiğit E, Mezarcıöz S, et al. Optimization of Coating Process Conditions for Denim Fabrics by Taguchi Method and Grey Relational Analysis[J]. J Nat Fibers 2020;19(2):685–99.
[21] Srinivasan VP, Palani PK, Balamurugan S. Experimental investigation on EDM of Si_3N_4–TiN using grey relational analysis coupled with teaching-learning-based optimization algorithm[J]. Ceram Int 2021;47(13):19153–68.
[22] Mohamed SAN, Zainudin ES, Sapuan SM, et al. Integration of Taguchi-Grey Relational analysis technique in parameter process optimization for rice husk composite[J]. Bio-Resources 2019;14(1):1110–26.
[23] Liu X, Tan H, Wang X, et al. Oxidation reactivity and kinetic analysis of bituminous coal char from high-temperature pyrolysis: Effect of heating rate and pyrolysis temperature[J]. Thermochim Acta 2020;690:178660.
[24] Wang Z, Zhang L, Zhao Y, et al. Experimental investigation on the evolution characteristics of anthracite-N and semi-coke reactivity under various O_2/H_2O pre-oxidation atmospheres[J]. Fuel Process Technol 2021;216:106725.
[25] Xu J, Su S, Sun Z, et al. Effects of steam and CO_2 on the characteristics of chars during devolatilization in oxy-steam combustion process[J]. Appl Energy 2016;182:20–8.
[26] Blaesing M, Mueller M. Release of alkali metal, sulphur, and chlorine species from high temperature gasification of high- and low-rank coals[J]. Fuel Process Technol 2013;106:289–94.
[27] Qi X, Song G, Yang S, et al. Migration and transformation of sodium and chlorine in high-sodium high-chlorine xinjiang lignite during circulating fluidized bed combustion[J]. J Energy Inst 2019;92(3):673–81.
[28] Gao Y, Chen Y, Li W, et al. Optimization Design of Centrifugal Pump Auxiliary Blades Based on Orthogonal Experiment and Grey Correlation Analysis[J]. Water 2023;15(13):2465.
[29] Zhang B, Tian Z, Wang Q, et al. Assessment of the impact of pyrolysis conditions on char reactivity through orthogonal experimental-based grey relational analysis[J]. J Anal Appl Pyrol 2024;179:106426.
[30] Zheng Z, You Y, Guo J, et al. Pyrolysis Behavior of Pyrite under a CO-H_2 Atmosphere[J]. ACS Omega 2022;7(33):29116–24.
[31] She Y, Zou C, Liu S, et al. Combustion and gasification characteristics of low-temperature pyrolytic semi-coke prepared through atmosphere rich in CH_4 and H_2[J]. Green Process Synth, 2021;10(1):189–200.
[32] Rezgui Y, Guemini M. Deactivation and Coke Formation on Nickel−Tungsten Supported on Silica−Alumina Catalysts[J]. Ind Eng Chem Res 2008;47(12):4056–62.
[33] Hu J, Qin Y, Li X, et al. Coupled Typical Coke Gasification and Sintering Ore Reduction in CO-N_2-H_2[J]. ACS Omega 2022;7(38):34420–7.
[34] Ma D, Li R, Wang X, et al. Chlorine evolution and char characteristics during pyrolysis upgrading of Xinjiang high chlorine coal[J]. Fuel 2025;379:133120.
[35] Yin H, Wang M, Wang J, et al. Effect of calcium and sodium additives on the pyrolysis characteristics of Pingshuo demineralized coal[J]. Clean Coal Technology 2010;3:31–5.
[36] Zhang Z, Zhang X, Zhang L, et al. Impacts of alkali or alkaline earth metals addition on reaction intermediates formed in methanation of CO_2 over cobalt catalysts[J]. J Energy Inst 2020;93(4):1581–96.
[37] Li CZ, Sathe C, Kershaw JR, et al. Fates and roles of alkali and alkaline earth metals during the pyrolysis of a victorian brown coal[J]. Fuel 2000;79(3):427–38.
[38] Ma R, Wei B, Fan W, et al. Research progress of sodium migration and transformation duringcombustion of Zhundong coals in China[J]. Clean Coal Technology 2023;29(10):27–53.
[39] Tu S, Zhang S, Shi D, et al. Effect of additive on emission of sodium in high-sodium coal during pyrolysis[J]. Coal Conversion 2016;39(1):31–4.
[40] Liu Y, Wang Z, Lyu Y, et al. Inhibition of sodium release from Zhundong coal via the addition of mineral additives: A combination of online multi-point LlBS and offline experimental measurements[J]. Fuel 2018;212(15):498–505.
[41] Guo S, Jiang Y, Xiong Q, et al. Release and transformation behaviors of sodium species with different occurrence modes during pyrolysis of Zhundong coal[J]. J Fuel Chem Technol 2017;45(3):257–64.
[42] Li X, Hayashi J, Li C. FT-Raman spectroscopic study of the evolution of char structure during the pyrolysis of a Victorian brown coal[J]. Fuel 2006;85(12–13):1700–7.
[43] Quyn DM, Wu H, Li C. Volatilisation and catalytic effects of alkali and alkaline earth metallic species during the pyrolysis and gasification of Victorian brown coal. Part I. Volatilisation of Na and Cl from a set of NaCl-loaded samples[J]. Fuel 2002;81(2):143–9.
[44] Stenberg VI, Jones MB, Suwarnasarn NJ. Radicals in coals during pyrolysis in relation to liquefaction conversion[J]. Fuel 1985;64(4):470–4.
[45] Chen S, Ding J, Li G, et al. Theoretical study of the formation mechanism of sulfur-containing gases in the CO_2 gasification of lignite[J]. Fuel 2019;242:398–407.
[46] Zhao D, Liu H, Sun C, et al. Combust Flame 2018;197:471–86.
[47] Yang J, Ma L, Yang J, et al. Chemical looping gasification of phosphogypsum as an oxygen carrier: The Ca and S migration mechanism using the DFT method[J]. Sci Total Environ 2019;689:854–64.
[48] Zheng L, Jin J, Zhang R, et al. Understanding the effect of dolomite additive on corrosion characteristics of straw biomass ash through experiment study and molecular dynamics calculations[J]. Energy 2023;271:126950.
[49] Nørskov JK, Bligaard T, Logadottir A, et al. Universality in Heterogeneous Catalysis [J]. J Catal 2002;209(2):275–8.
[50] Zhang L, Sun R, Wang Z, et al. Application of experiments and density function theory on the formation mechanism of NH_3 during O_2/Ar and O_2/H_2O combustion process of demineralized coals[J]. Fuel 2023;331(1):125730.
[51] Liu J, Zhang X, Hu B, et al. Formation mechanism of HCN and NH3 during indole pyrolysis: A theoretical DFT study[J]. J Energy Inst 2020;93(2):649–57.
[52] Liu S, Xiang D, Xu Y, et al. Relationship between electronic properties of Fe_3O_4 substituted by Ca and Ba and their reactivity in chemical looping process: A first-principles study[J]. Appl Energy 2017;202:550–7.
[53] Hosseini D, Donat F, Kim SM, et al. Redox-driven restructuring of FeMnZr-oxygen carriers enhances the purity and yield of H_2 in a chemical looping process [J]. ACS Appl Energy Mater 2018;1(3):1294–303.